Electronic Supplementary Material (ESI) for ChemComm.

" *Correlating the induced zero field splitting with the slow relaxation of the magnetization in Gd^{III} SIMs* "

Júlia Mayans,[*a] Albert Escuer[b]

[a] Instituto de Ciencia Molecular (ICMol), Universitat de València, 46980 Paterna (València), Spain. E-mail: julia.mayans@uv.es

b Departament de Química Inorgànica i Orgànica, Secció Inorgànica and Institute of Nanoscience (IN2UB) and Nanotecnology, Universitat de Barcelona, Martí i Franquès 1-11, Barcelona-08028, Spain

1-Instrumental measurements

IR spectra (4000-400 cm-1) were recorded using a Bruker IFS-125 FT-IR spectrometer with samples prepared as KBr pellets. Variable-temperature magnetic studies were performed using a MPMS-5 Quantum Design magnetometer operating at 0.03 T in the 300-2.0 K range. Magnetization measurements were performed in the 0-5 T fields. X-Band EPR spectra of polycrystalline samples were recorded at 4 K with a Bruker ER 200 spectrometer equipped with a helium continuous-flow cryostat. Diamagnetic corrections were applied to the observed paramagnetic susceptibility using Pascal's constants. Fits of the magnetic data (susceptibility, magnetization and EPR simulation) were performed with PHI software. Powder X-ray diffraction was performed with a PANalytical X'Pert PRO MPD θ/θ powder diffractometer of 240 millimetres of radius, in a configuration of convergent beam with a focalizing mirror and a transmission geometry with flat samples sandwiched between low absorbing films and Cu $K\alpha$ radiation (λ = 1.5418 Å). ECD spectra were recorded in methanolic solutions in a Jasco-815 spectropolarimeter.

2-Syntheses and characterization.

All reactions were performed in an Anton Paar Monowave 300 microwave furnace in a 30 mL glass closed vial with continuous stirring according the following scheme for both enantiomers (*R*, *R*) and (*S*, *S*):

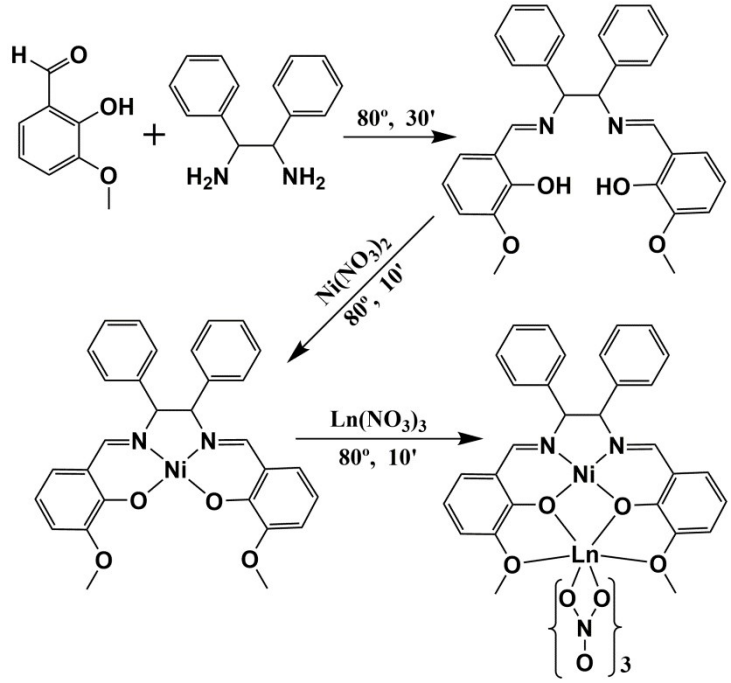

Complex [NiGd(L)$(NO_3)_3$] (1). A solution of 0.053 g (0.25 mmol) of (*R*,*R*) or (*S*,*S*)-diphenylehylendiamine and 0.076 g (0.5 mmols) of 2-hydroxy-3-methoxybenzaldehyde were dissolved in 20 mL of methanol and heated at 80º C during 30 minutes. To the resulting yellow solution solid nickel nitrate hexahydrate (0.073 g, 0.25 mmol) was added and the mixture was heated at 80 º C during 10 minutes, resulting a red solution of the nickel precursor. After addition of solid gadolinium nitrate (0.113 g, 0.25 mmol) the solution was heated 10 minutes at 80º and cooled to room temperature. Complex 1 precipitates as a red powder in high yield (90 %).

Complex [$NiEu_{0.85}Gd_{0.15}$(L)$(NO_3)_3$] (2). The synthesis was performed following the same procedure but adding in the third step 0.200 mmol of europium nitrate hexahydrate and 0.050 mmols of gadolinium nitrate hexahydrate. The solid was collected as a red powder in a similar yield. Anal. calculated/found (%): for **1**, C, 40.9/40.7; H 2.97/3.0; N 9.95/9.8; for **2**, C, 41.1/40.9; H 2.99/2.8; N 7.99/8.1; Infrared spectra are shown in Fig. S1.

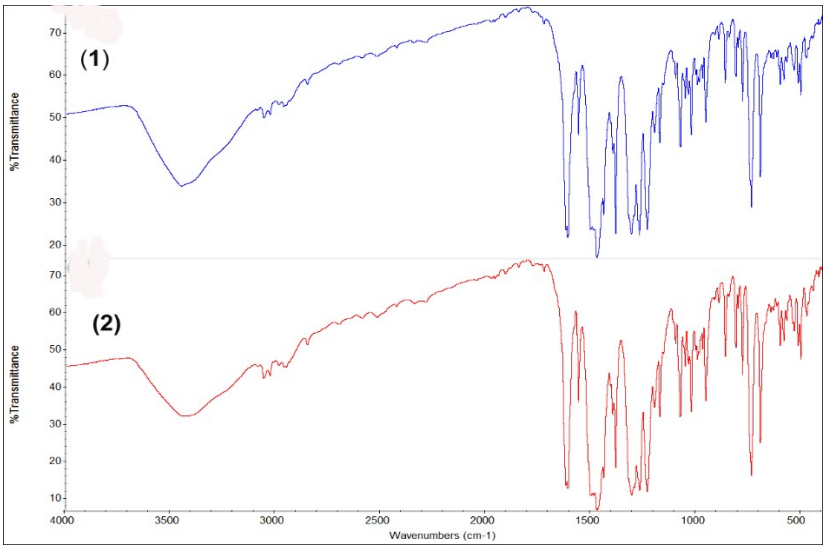

Fig. S1. Infrared spectra for the complexes **1** and **2**.

The (*R*,*R*) and (*S*,*S*) enantiomers of complex **1** were characterized. The spectra are identical to the previously reported for the Eu^{III} complex (reference XX in the main text). The differences for the square planar Ni^{II} cations between both enantiomers are negligible and even the gadolinium cations become chiral centres, the differences in its coordination sphere are mainly limited to the relative position of the nitrato ligands. Electronic circular dichroism (ECD) spectra in methanolic solution were performed for the enantiomeric pair of (*R*,*R*) and (*S*,*S*)-**1** complexes, providing an additional prove of its identity in solution, Fig. S2. The mirror image spectrum for the $Ni^{II}Gd^{III}$ complexes confirms its enantiomeric nature and exhibits positive Cotton effect at λ_{max} = 565(w), 461(sh), 410(st), 370(sh) 273(st), 245(w) and 221(st) nm and negative bands at 486(vw), 325(m) and 207(st) nm for **1*RR*** and the same set of bands with opposite sign for **1*SS*** mainly due to the chiral ligands.

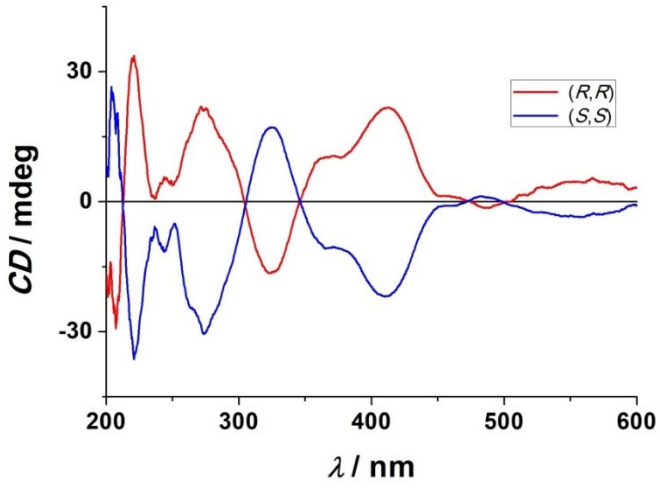

Fig. S2. Solution ECD spectra for the $Ni^{II}Gd^{III}$ pair of complexes **1*RR*** and **1*SS***. (*R*,*R*) enantiomer, red line; (*S*,*S*) enantiomer, blue line.

3-Structural aspects.

Powder X-ray diffraction of the [NiGd(L)$(NO_3)_3$] (**1**) and the [$NiGd_xEu_{1-x}$(L)$(NO_3)_3$] (**2**) complexes (Fig. S3), demonstrates its isostructurality with the structure of [NiEu(L)$(NO_3)_3$] complex, Fig. S4. Complete description of the molecular features of the Eu^{III} complex can be found in our previous previously reported paper *Dalton Trans.* **2019**, *48*, 641-652, CCDC code: JIWNAH/JIWNEL for both enantiomers.

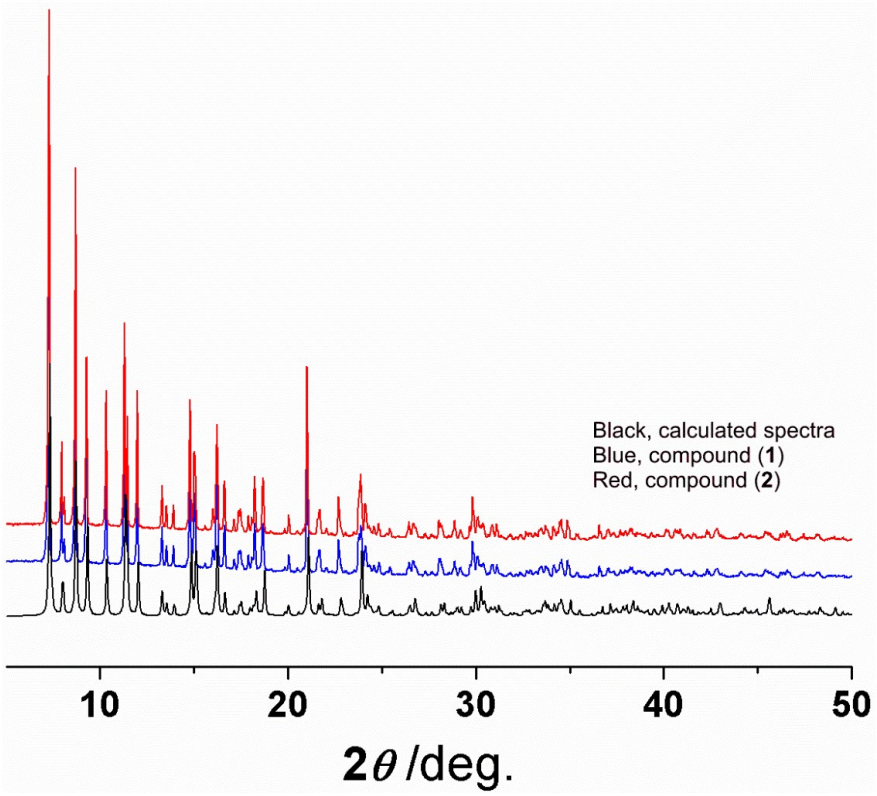

Fig. S3. Powder X-ray diffraction spectra for the [NiEuL$(NO_3)_3$] reference complex calculated from the single crystal diffraction data of the previously reported structure JIWNAH (black) and complexes **1** (blue) and **2** (red) showing its isostructurality.

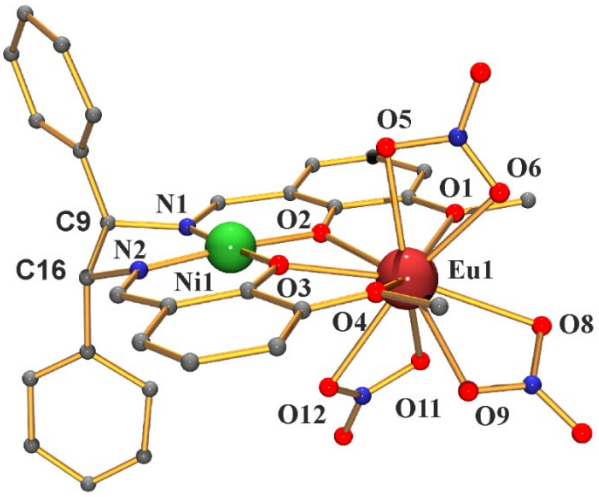

Fig. S4. Partially labelled plot for the reference complex [NiEuL$(NO_3)_3$].

For the purposes of this work the most important features are those related with the intermolecular interactions and the distance to the neighbors.

The Ni^{II} cation is tetracoordinated (square planar) with bond distances of 1.806-1.843 Å, typical of this coordination. The Eu^{III} cation exhibits a decacoordinated environment with bond distances completes its coordination sphere with three bidentate nitrato ligands, being the bond distances Eu^{III}-O(nitrate) > Eu^{III}-O(methoxy) > Eu^{III}-O(phenoxo), Table S1. SHAPE calculations indicate that the coordination polyhedron around the Ln^{III} cation is close to an ideal sphenocorona (C_{2v}, CShM = 3.24), distorted due to the low bite of the bidentate nitrato ligands.

Table S1 Selected bond distances (Å) and angles (º) for the reference complex [NiEuL$(NO_3)_3$] extracted from *Dalton Trans.* **2019**, *48*, 641-652.

Eu(1)-O(1)	2.552(7)	Ni(1)-N(1)	1.806(7)
Eu(1)-O(2)	2.389(6)	Ni(1)-N(2)	1.840(6)
Eu(1)-O(3)	2.417(4)	Ni(1)-O(2)	1.838(6)
Eu(1)-O(4)	2.550(6)	Ni(1)-O(3)	1.843(6)
Eu(1)-O(5)	2.504(6)	Ni(1)-O(2)-Eu(1)	106.7(3)
Eu(1)-O(6)	2.421(5)	Ni(1)-O(3)-Eu(1)	105.4(2)
Eu(1)-O(8)	2.593(6)	Ni(1)···Eu(1)	3.406(1)
Eu(1)-O(9)	2.480(6)		
Eu(1)-O(11)	2.472(6)		
Eu(1)-O(12)	2.538(5)		

The molecules are well isolated without solvent molecules that could interact with the complexes. The main intermolecular interactions consist of very weak CH-π(ring) contacts, Fig. S5, that promote chains of clusters in the network. The interaction is established between one H-atom of one of the methyl groups of the L^{2-} ligands which is directed towards the centroid of one phenyl group of the neighbouring molecule.

On this basis, the Ln^{III} cations are very well isolated and the only interactions are those derived of the dipolar contacts from the three neighboring clusters placed at around 8 A.

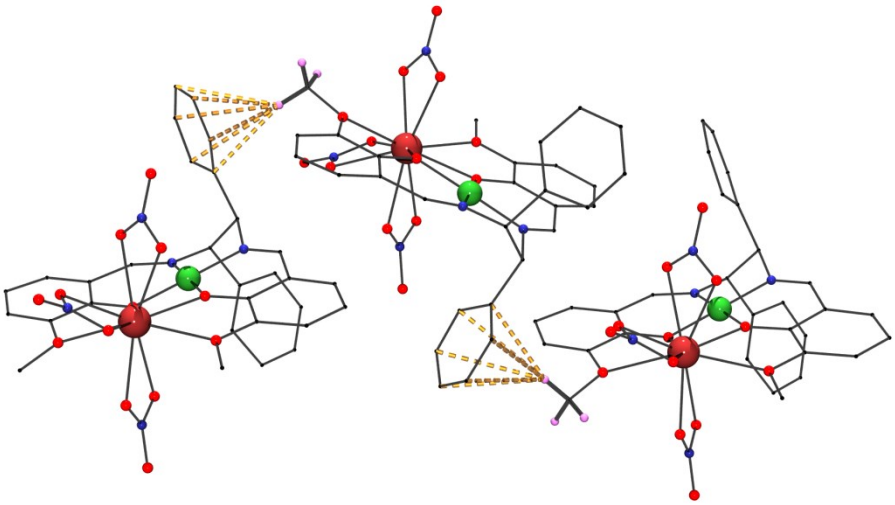

Fig. S5. CH-π(ring) interactions between the dinuclear [$Ni^{II}Ln^{III}$] complexes. This weak interactions, that determines its 1-D arrangement of dimers, are the only intermolecular contacts. (extracted the CCDC structure JIWNAH).

4-Magnetic data.

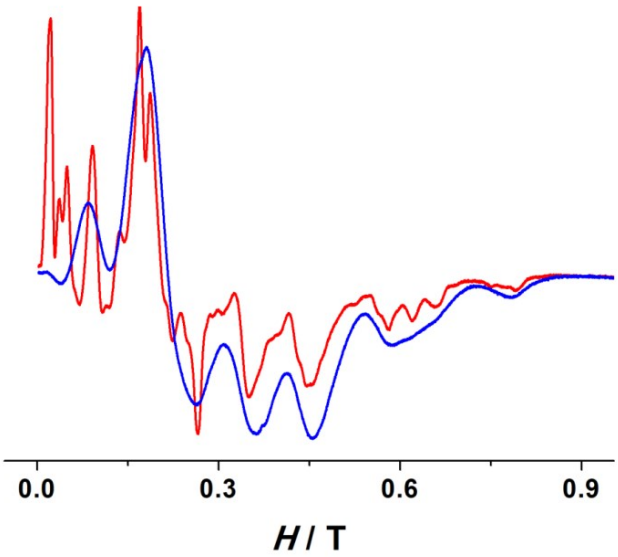

Fig. S6. *X*-band EPR spectrum recorded at 4 K for complex **1** (blue line) and the diluted complex **2** (red line), showing the same bands (better defined for **2**), reflecting the same environment and *D* value. The EPR spectra has been simulated using PHI software. [1]

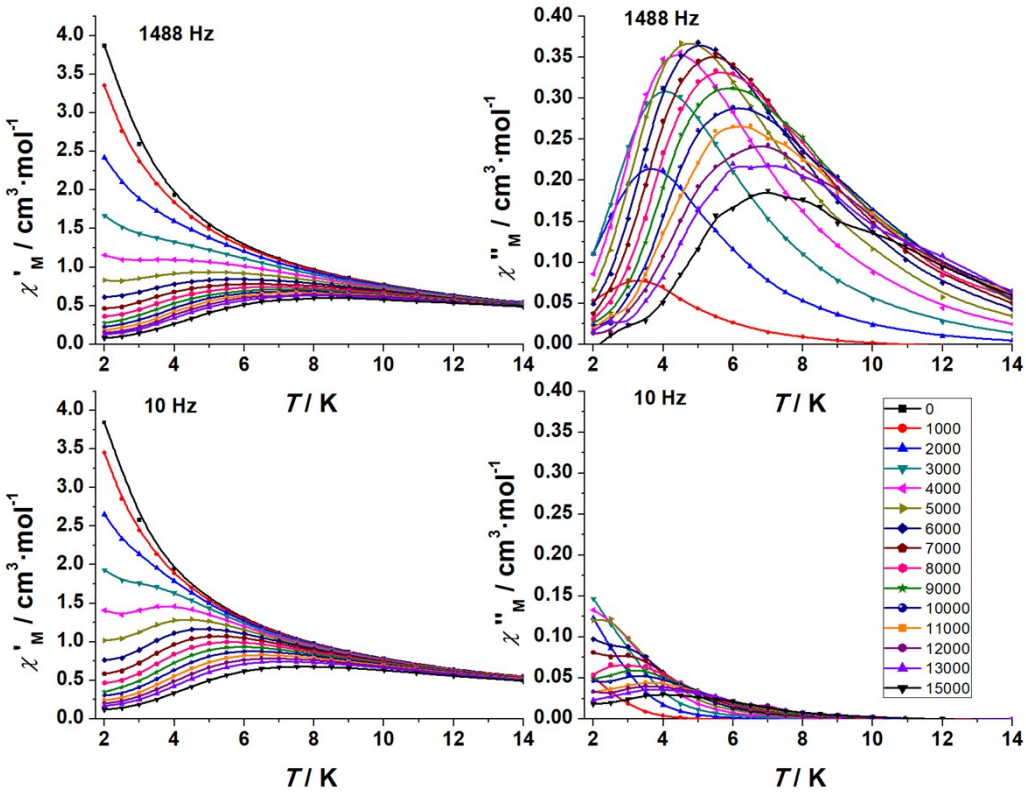

Fig. S7. $\chi''_M T$-*f*(T) plots measured under different transverse fields between 0 – 1.5 T for complex **1** for two LF and HF frequencies.

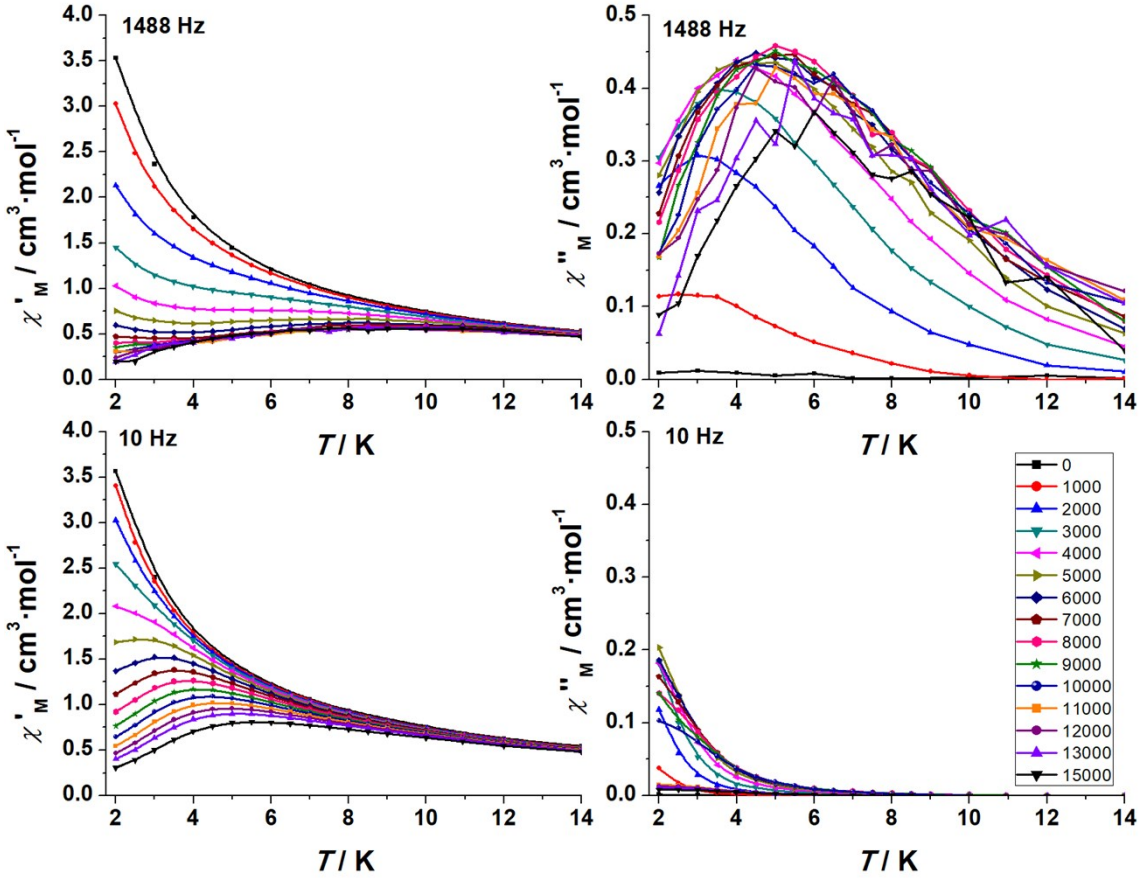

Fig. S8. $\chi''_M T$-f(T) plots measured under different transverse fields between 0 – 1.5 T for complex **2** for two LF and HF frequencies.

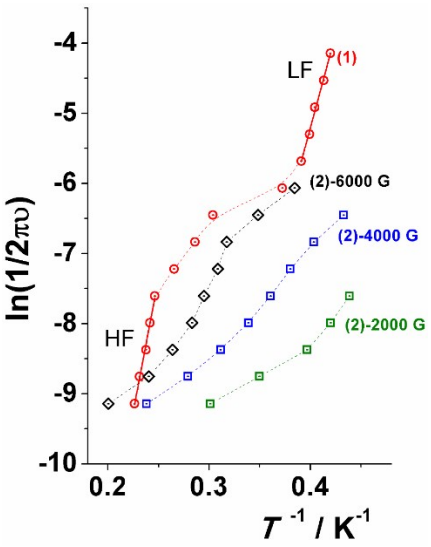

Fig. S9. Plot of ln(1/2πν) vs. T^{-1} for the referenced compounds and transverse fields. The values in the graph have been extracted of the maxima in the χ'' vs T plots.

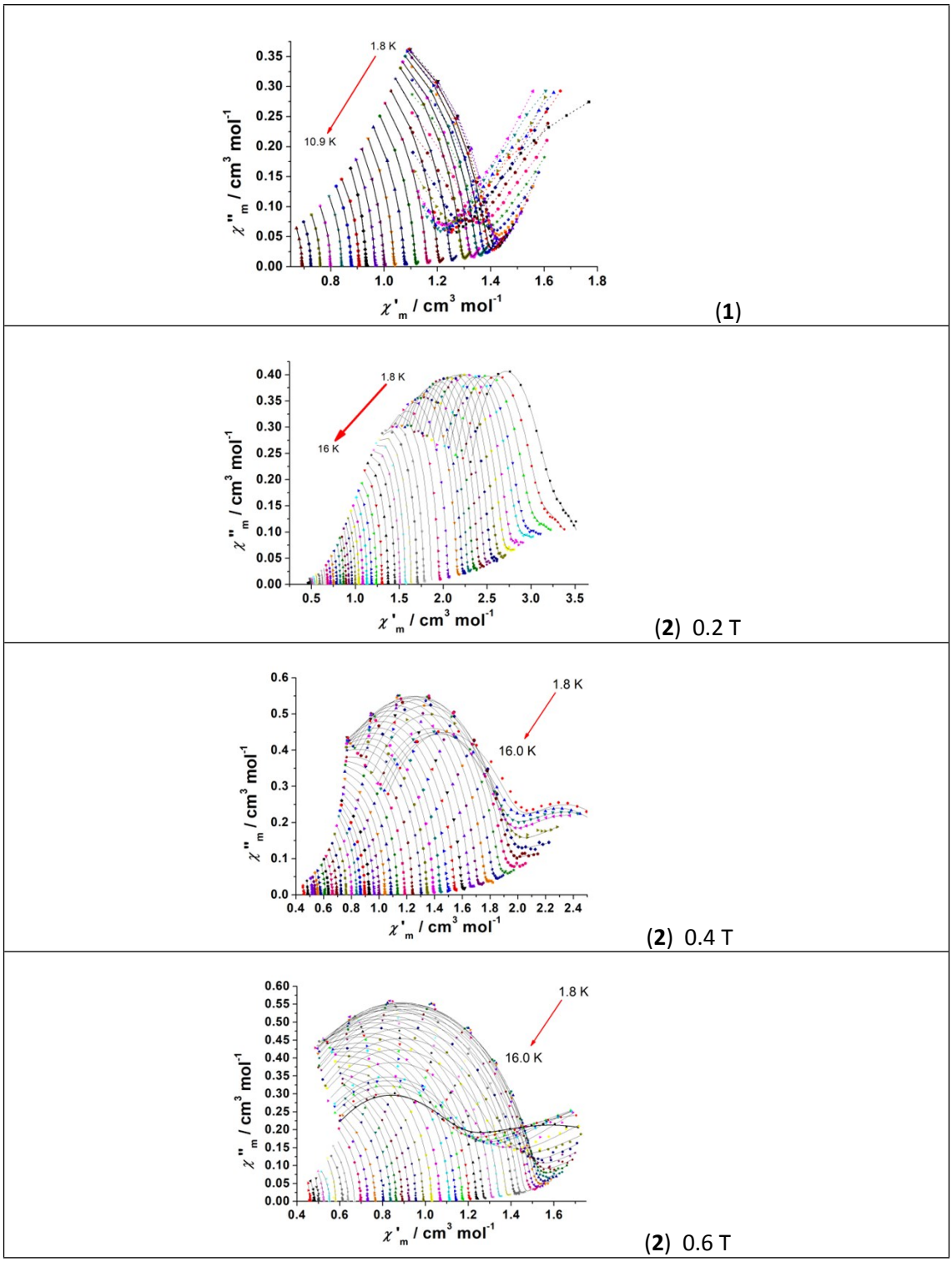

Fig. S10. Argand plots for the references complexes and different *dc* fields. Solid lines show the fit of the experimental data.

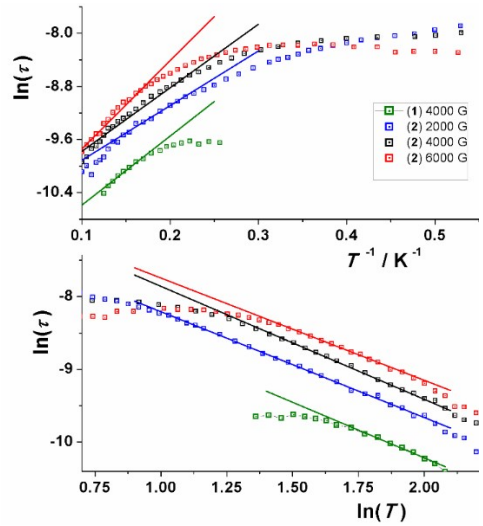

Fig. S11. Top, ln(τ) vs. T^{-1} fitted according ln(τ) = ln(τ_0) + (U_{eff}/kT) and bottom ln(τ) *vs*. (T) fitted according ln(τ) = ln(a) +n ln(T). The values of τ have been extracted from the fitting of the Argand plots according to Debye model using CCfit software.

Table S2. Fit parameters corresponding to the above Fig. S11.

Compound	Dc field (T)	lna	n	τ_0 (s)	U_{eff} (K)
1	0.4	-7.166	1.53	$8.9\cdot10^{-6}$	10.40
2	0.2	-6.756	1.45	$1.65\cdot10^{-5}$	9.68
2	0.4	-6.309	1.55	$2.19\cdot10^{-5}$	9.56
2	0.6	-6.40	1.40	$1.54\cdot10^{-5}$	13.33

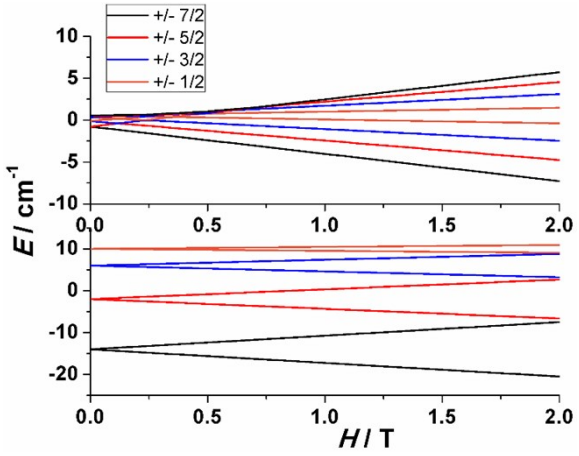

Fig. S12. Top, axial Zeeman plot for a S = 7/2 and D = -0.11 cm^{-1} showing the crossing of the m_s levels for low dc fields. Bottom, Zeeman plot for a hypothetic D value of 2 cm^{-1} for which conventional double-well processes could be possible.

1. N. F. Chilton, R. P. Anderson, L. D. Turner, A. Soncini and K. S. Murray *J. Comput. Chem.*m *2013*, **34**, 1164.